AIAA 82-4259

Numerical Simulation of the Inhomogeneous Discharge Structure in Noble Gas MHD Generators

T. Hara,* A. Veefkind,† and L. H. Th. Rietjens†
Eindhoven University of Technology, Eindhoven, the Netherlands

A numerical calculation has been developed to describe the two-dimensional, time-dependent behavior of an inhomogeneous plasma in nonequilibrium MHD generators. The development of "streamers" as typical discharge structures is simulated. A cesium-seeded argon plasma is considered. The numerical conditions used in the calculations are set equal to the experimental conditions used in the Eindhoven shock-tube facility. The elliptic part of the equations is solved by the finite-element method and the hyperbolic part by integration along the characteristic lines. It is found that the current concentrations on each electrode edge grow within microseconds into discharge structures which are concentrated in nonstationary streamers transverse to the gas flow. After they are formed, these streamers are frozen in the gas and are convected downstream at the gas velocity. Inside the streamers the cesium is fully ionized and the electron temperature is in range of 4000-6000 K, and outside the streamers the electron density is about 10^{19} and the electron temperature is about 2500 K. These calculated results agree quite well with the experimental ones observed in the Eindhoven shock-tube facility.

Nomenclature

$\boldsymbol{B}$ = magnetic induction
$\mathcal{E}_i$ = ionization potential
$\boldsymbol{E}$ = electric field
$\boldsymbol{E}^*$ = induced electric field
e = charge of the electron
h = channel height
I_L = load current
j = current density
K = load factor of a generator
k = Boltzmann constant
k_f, k_r = ionization and recombination rate coefficient, respectively
M = flow Mach number
m_e = mass of an electron
m_j = mass of species j
N = interpolation function
n_e, n_s = electron and seed density, respectively
P_d = electrical output density of a generator
p_e, p_s = electron and stagnation pressure, respectively
Q_j = momentum transfer cross section of electrons with species j
Q_r = radiation loss
q_e = electron heat flux
s = electrode pitch
s_f = seed ratio
T = heavy species temperature
T_e, T_s = electron and stagnation temperature, respectively
t = time
$\boldsymbol{u}$ = heavy species flow velocity
$\boldsymbol{u}_e$ = electron drift velocity
V_L = load voltage
w = channel width
β = Hall parameter
β_{eff} = effective Hall parameter
ν_j = collision frequency of electrons and species j
σ = electrical conductivity
σ_{eff} = effective electrical conductivity
$\tau_{ne,\text{ relax}}$ = relaxation time of electron density
$\tau_{Te,\text{ relax}}$ = relaxation time of electron temperature
ψ = current stream function

Received May 11, 1981; revision received Jan. 27, 1982.

*Visiting Scientist; Associate Professor, Department of Electrical Engineering, Kyoto University, Kyoto, Japan.

†Staff Member, Group Direct Energy Conversion, Department of Electrical Engineering.

Introduction

SHOCK-tube experiments as well as experiments in continuous MHD generator flows of seeded gases show a strongly nonuniform discharge structure.[1-3] The observed streamers can be explained as the result of nonlinear growth of ionization instabilities.[4] Because of the strong nonuniformity of the discharges a quantitative description cannot follow from a linear or a quasilinear instability theory.[5,6] The influence of strong nonuniformity on the electrical behavior of the gas can be described by considering statistical characteristics of the fluctuations as a preassumption.[7,8] For the description of the development of ionization instabilities in the MHD channel, numerical simulation studies are of importance. These calculations are carried out in the nonlinear domain and take into account the boundary conditions of the duct. Lengyel[9] and Velikov[10] have found numerically the inhomogeneous structures in nonmoving plasmas. Uncles[11] has studied the more realistic case where the convection term is included.

The aim of this study is to explain the inhomogeneous discharge structure as observed in the Eindhoven shock-tube facility as the result of nonlinear growth of ionization instabilities by numerical simulation of the plasma. A two-dimensional, time-dependent numerical model is used. The set of governing equations consists of two parts, one elliptic and the other hyperbolic. The elliptic part is solved by the finite-element method[12] and the hyperbolic part by integration along the characteristic lines. The finite-element method in which the physical model is represented by elements has the advantage in dealing with the convection term over the finite-difference method in which the physical model is represented by points. Careful estimation of the characteristic relaxation time of the electron density and temperature is important in determining the space and time steps in the calculation.

Theoretical Model

Basic Equations

In studies of the stability and discharge structure of nonequilibrium, partially ionized plasmas, it is frequently sufficient to consider the heavy particle properties as prescribed and constant in space and time. In this limit the governing equations of the Ar-Cs plasma are given by the following set

$$j+\frac{\beta}{B}(j\times B)=\sigma\left(E^*+\frac{\nabla p_e}{n_e}\right) \tag{1a}$$

$$\nabla\cdot j=0 \tag{2}$$

$$\nabla\times E=0 \tag{3}$$

$$\frac{\partial n_e}{\partial t}+\nabla\cdot(n_e u_e)=k_f n_e(n_s-n_e)-k_r n_e^3=\dot{n}_e \tag{4a}$$

$$\frac{\partial}{\partial t}\left\{n_e\left(\frac{3}{2}kT_e+\mathcal{E}_i\right)\right\}+\nabla\cdot\left\{n_e\left(\frac{3}{2}kT_e+\mathcal{E}_i\right)u_e\right\}$$
$$=j\cdot E^*-\nabla\cdot(p_e u_e)-\frac{3}{2}\delta n_e m_e k(T_e-T)\sum_{j=1}^{3}\frac{\nu_j}{m_j}$$
$$-\nabla\cdot q_e-Q_R \tag{5a}$$

where

$$\sigma=e^2 n_e/m_e\nu_e \tag{6}$$

$$\beta=eB/m_e\nu_e \tag{7}$$

$$E^*=E+u\times B \tag{8}$$

$$p_e=n_e kT_e \tag{9a}$$

$$j=n_e e(u-u_e) \tag{10}$$

$$k_r=1.09\times10^{-20}T_e^{-9/2} \tag{11}$$

$$k_f=2.42\times10^{21}k_r T_e^{3/2}\exp(-\mathcal{E}_i/kT_e) \tag{12}$$

$$\nu_j=n_j Q_j(8kT_e/\pi m_e)^{1/2} \tag{13}$$

$$\nu_e=\sum_{j=1}^{3}\nu_j \tag{14}$$

$j=1$, 2, or 3 denotes argon atoms, cesium atoms, and cesium ions, respectively. The electron-atom cross sections for argon and cesium are taken $0.280\times10^{-20}(1.46\times10^{-3}T_e-0.535)$ m^2 and 0.5×10^{-17} m^2, respectively. The electron-ion collision cross section is taken from Spitzer.[13] $\nabla\cdot q_e$ and Q_R are the heat conduction and radiation loss, respectively.

In these equations, only single ionization of cesium by electron-atom collisions and three-body recombinations are considered. Charge neutrality and low magnetic Reynolds number are also assumed.

Further Assumptions

We shall further make the following assumptions:

1) The heavy particle velocity has the form $u=(u, 0, 0)$.

2) The magnetic field has the form $B=(0, 0, B)$.

3) All quantities are constant in the z direction,

$$\frac{\partial}{\partial z}=0 \tag{15}$$

4) The term $\nabla p_e/n_e e$ in Ohm's law is neglectable.

Equation (1a) then reduces to

$$E_x^*=(1/\sigma)(j_x+\beta j_y),\qquad E_y^*=(1/\sigma)(-\beta j_x+j_y) \tag{1b}$$

where,

$$E_x^*=E_x,\qquad E_y^*=E_y-uB \tag{9b}$$

Using the above assumptions, the electron continuity and electron energy equations are reduced to the following set:

$$\frac{1}{n_e}\frac{\partial n_e}{\partial t}=\frac{\dot{n}_e}{n_e}-\frac{u}{n_e}\frac{\partial n_e}{\partial x} \tag{4b}$$

$$\frac{1}{T_e}\frac{\partial T_e}{\partial t}=\frac{2}{3kn_eT_e}\frac{j_x^2+j_y^2}{\sigma}-\delta m_e\left(1-\frac{T}{T_e}\right)\sum_{j=1}^{3}\frac{\nu_j}{m_j}$$
$$-\left(1+\frac{2\mathcal{E}_i}{3kT_e}\right)\frac{\dot{n}_e}{n_e}-\frac{2}{3}\frac{u}{n_e}\frac{\partial n_e}{\partial x}-\frac{5}{3}\left(u-\frac{j_x}{n_e e}\right)\frac{1}{T_e}\frac{\partial T_e}{\partial x}$$
$$+\frac{5}{3}\frac{j_y}{n_e e}\frac{1}{T_e}\frac{\partial T_e}{\partial y}-\frac{2}{3}\frac{\nabla\cdot q_e}{kn_eT_e}-\frac{2}{3}\frac{Q_R}{kn_eT_e} \tag{5b}$$

Moreover, in Eq. (5b) we will neglect all terms including space derivatives and the radiation term Q_R with respect to the first three terms. Then Eq. (5b) becomes

$$\frac{1}{T_e}\frac{\partial T_e}{\partial t}=\frac{2}{3kn_eT_e}\frac{j_x^2+j_y^2}{\sigma}-\delta m_e\left(1-\frac{T}{T_e}\right)\sum_{j=1}^{3}\frac{\nu_j}{m_j}$$
$$-\left(1+\frac{2\mathcal{E}_i}{3kT_e}\right)\frac{\dot{n}_e}{n_e} \tag{5c}$$

The validity of these assumptions is checked after the solution has been obtained.

Gasdynamic and Geometrical Conditions

The gasdynamic conditions used in the calculations are taken equal to experimental values obtained in the Eindhoven shock-tube facility: stagnation temperature $T_s=2000$ K, Mach number $M=1.6$, static pressure $p_s=1.2$ atm, magnetic field $B=3$ T, load resistance $R_L=2\Omega$, and seed fraction $s_f=2\times10^{-4}$. From these conditions it follows that the gas temperature $T=1079$ K, the gas velocity $u=980$ m/s, the argon number density $n_A=8.16\times10^{24}$ m^{-3}, and the cesium number density $n_s=1.63\times10^{21}$ m^{-3}.

The dimensions of the channel have been chosen equal to two-fifths of the dimensions of an actual Faraday channel: the channel height $h=40$ mm, the channel width $w=40$ mm, one pitch length $s=10$ mm, and the electrode width $c=4$ mm. One section of the segmented electrode Faraday channel is shown in Fig. 1.

Stream Function

Equation (2) permits the representation of j in terms of a current stream function defined by

$$j_x=\frac{\partial\psi}{\partial y},\qquad j_y=-\frac{\partial\psi}{\partial x} \tag{16}$$

An equation for ψ is developed using Eqs. (16) and (3) and the relation $\nabla\times(u\times B)=0$

$$\nabla\times E^*=\frac{\partial}{\partial x}\left\{\frac{1}{\sigma}\left(-\frac{\partial\psi}{\partial x}-\beta\frac{\partial\psi}{\partial y}\right)\right\}$$
$$-\frac{\partial}{\partial y}\left\{\frac{1}{\sigma}\left(\frac{\partial\psi}{\partial y}-\beta\frac{\partial\psi}{\partial x}\right)\right\}=0 \tag{17}$$

At the electrodes the electrical boundary condition is

$$E_x = 0 \tag{18a}$$

Substitution in Ohm's law and application of Eq. (16) yields

$$\frac{\partial \psi}{\partial y} - \beta \frac{\partial \psi}{\partial x} = 0 \tag{18b}$$

The electrical boundary condition at the insulators is

$$j_y = 0 \tag{19a}$$

or

$$\psi = \text{const} \tag{19b}$$

By definition ψ is taken equal to zero at the left insulator. Then $\psi(AB) = \psi(EF) = 0$ and $\psi(CD) = \psi(GH) = I_L/w$ where I_L is the load current (see Fig. 1).

Periodicity is assumed over the one pitch length s

$$j(s,y) = j(0,y) \tag{20a}$$

or

$$\psi(s,y) = \psi(0,y) + I_L/w \tag{20b}$$

Numerical Procedure

Basic Procedure

After the application of the assumptions to the basic equations, the set of equations to be solved consists of Eqs. (1b), (16), (17), (4b), and (5c). Because the character of the set of equations is of the elliptic-hyperbolic type it is obvious, for solution purposes, to divide the set into an elliptic and hyperbolic part. At $t<0$ the plasma is assumed to be in Saha equilibrium with the electron temperature equal to the stagnation gas temperature. At $t=0$ the electrodes are connected to the external circuits, and the resulting current or potential distribution is solved from Eqs. (1b), (16), and (17) which form an elliptic set. Having found the current of potential distribution, the n_e and T_e distributions at the next time step can be found by integrating Eqs. (4b) and (5c) which form a hyperbolic set along their characteristics. This procedure is repeated for sequential time steps.

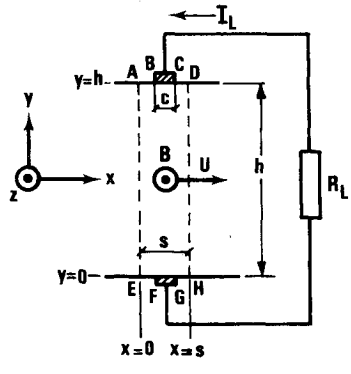

Fig. 1 Section of a segmented electrode Faraday channel.

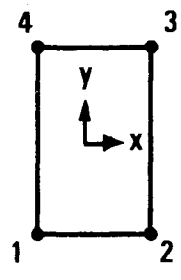

Fig. 2 A rectangular element.

Elliptic Part

From a known n_e and T_e distribution the current distribution is solved by using a finite-element method. The one-pitch region S (ADHE) shown in Fig. 1, in which the current distribution is to be calculated, is divided into small rectangular elements. Within one element having the nodes 1, 2, 3, 4 in space defined by the x,y coordinates shown in Fig. 2, we shall assume that n_e and T_e and hence σ and β are constant and that the stream function $\psi(x,y)$ is given by

$$\psi^e(x,y) = \{N(x,y)\}^T \{\Psi^e\} \tag{21}$$

where

$$[N(x,y)]^T = [N_1(x,y) \cdots \cdots N_4(x,y)] \tag{22a}$$

and

$$\{\Psi^e\} = \begin{Bmatrix} \psi_1 \\ \vdots \\ \psi_4 \end{Bmatrix} \tag{22b}$$

in which ψ_i represents the value of ψ at node i, and $N_i(x,y)$ is an interpolation function expressed by

$$N_i(x,y) = a_i + b_i x + c_i y + d_i xy \tag{23}$$

in which the coefficients a_i, b_i, c_i, and d_i can be determined by the coordinates of the four nodes of the element.

From the Galerkin process, the value of ψ of every node is determined so that they satisfy the next set of equations, namely Eqs. (19b) and (20b) and the following weighted

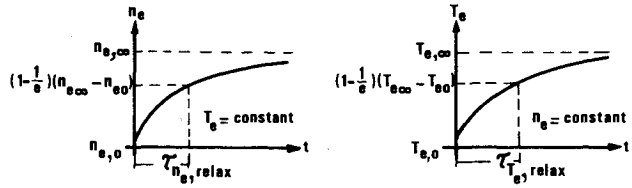

Fig. 3 Definition of the relaxation times, $\tau_{ne,\text{relax}}$ and $\tau_{Te,\text{relax}}$ of the electron density and the electron temperature.

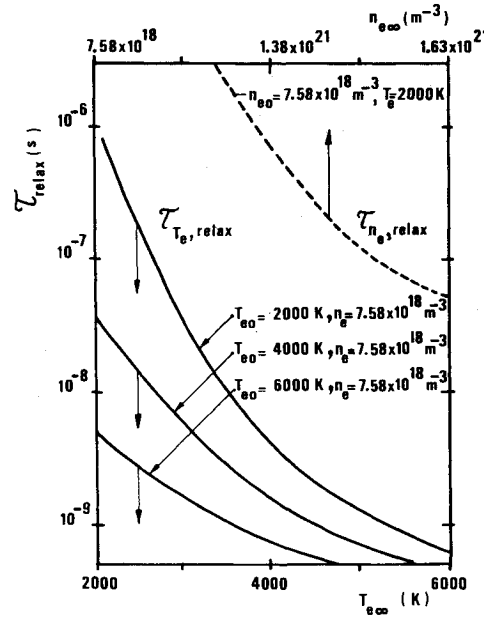

Fig. 4 The relaxation time $\tau_{ne,\text{relax}}$ for $n_{e0} = 7.58\times10^{18}$ m^{-3} as a function of $n_{e\infty}$ at $T_e = 2000$ K and the relaxation time $\tau_{Te,\text{relax}}$ as a function of $T_{e\infty}$ at $n_e = 7.58\times10^{18}$ m^{-3} (the upper and lower horizontal scales are related in such a way that $n_{e\infty}$ is the Saha value at the corresponding $T_{e\infty}$).

integral of Eq. (19a) over the one-pitch region S,[12]

$$\iint_S N_i(\nabla \times E_i^*)\,dxdy = 0 \tag{24}$$

Equation (24) must be established for every node i in region S except the nodes on AB, CD, EF, GH, AE, and DH in Fig. 1. Applying the Gauss theorem to Eq. (24) yields

$$\iint_S \left(\frac{\partial N_i}{\partial y}E_x^* - \frac{\partial N_i}{\partial x}E_y^*\right)dxdy + \oint_C (N_i E_y^* dy - N_i E_x^* dx) = 0 \tag{25}$$

where C = AEHDA. Since i is not the node on AB, CD, EF, GH, AE, and DH, $N_i = 0$ on AB, CD, EF, GH, AE, and DH in Eq. (25). The second term of Eq. (25) then reduces to

$$\int_B^C N_i E_x^* dx - \int_G^F N_i E_x^* dx$$

Moreover, from Eqs. (18) and (9b), $E_x^* = E_x = 0$ (on BC and FG) so that Eq. (25) becomes

$$\iint_S \left(\frac{\partial N_i}{\partial y}E_x^* - \frac{\partial N_i}{\partial x}E_y^*\right)dxdy = 0 \tag{26}$$

substituting Eqs. (1b) and (16) into Eq. (26) yields

$$\iint_S \left[\frac{1}{\sigma}\left\{\frac{\partial N_i}{\partial x}\left(\frac{\partial \psi}{\partial x} + \beta\frac{\partial \psi}{\partial y}\right) + \frac{\partial N_i}{\partial y}\left(\frac{\partial \psi}{\partial y} - \beta\frac{\partial \psi}{\partial x}\right)\right\}\right]dxdy = 0 \tag{27}$$

Dividing the region S in Eq. (27) in elements, and using Eq. (21), we get finally

$$\sum_{\text{all elements}} [K^e]\{\Psi^e\} = 0 \tag{28}$$

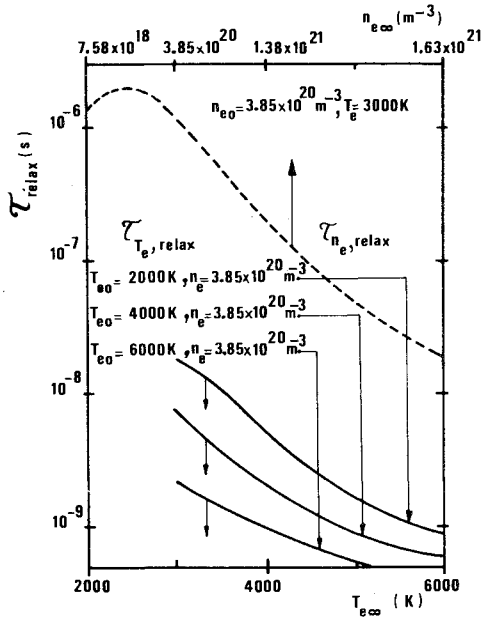

Fig. 5 The relaxation time $\tau_{ne,relax}$ for $n_{e0} = 3.58 \times 10^{20}$ m^{-3} as a function of $n_{e\infty}$ at $T_e = 3000$ K and the relaxation time $\tau_{Te,relax}$ as a function of T_e at $n_e = 3.58 \times 10^{20}$ m^{-3} (the upper and lower horizontal scales are related in such a way that $n_{e\infty}$ is the Saha value at the corresponding $T_{e\infty}$).

where

$$[K_e] = \iint_{S^e} \frac{l}{\sigma}(\{N_x\}\{N_x\}^T + \beta\{N_x\}\{N_y\}^T - \beta\{N_y\}\{N_x\}^T + \{N_y\}\{N_y\}^T)\,dxdy \tag{29}$$

(4×4)

in which S^e is the area of each element and N_x and N_y means $\partial N/\partial x$ and $\partial N/\partial y$, respectively.

By solving the set of simultaneous equations, Eq. (28) together with Eqs. (19a) and (19b), we finally obtain the values of ψ at every node and then from Eq. (16) the current density j can be calculated. The one-pitch region is divided into $40 \times 10 = 400$ elements ($\Delta x = 0.25$ mm, $\Delta y = 4.0$ mm). Since the convergence of the solution of the simultaneous equation is very slow by the conventional successive over-relaxation (SOR) method in our high β case ($\beta \simeq 16$ at $t = 0$), the direct inversion method has been applied.

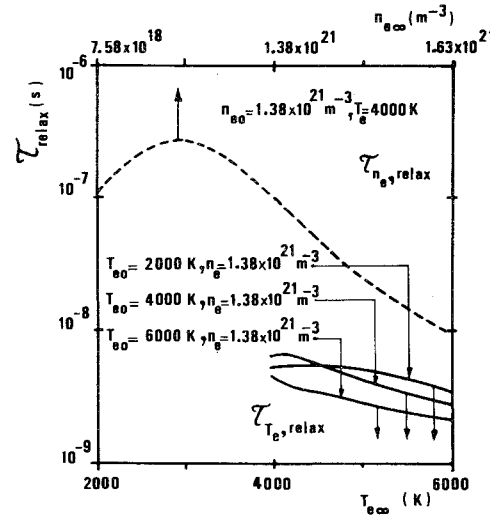

Fig. 6 The relaxation time $\tau_{ne,relax}$ for $n_{e0} = 1.38 \times 10^{21}$ m^{-3} as a function of n_e at $T_e = 4000$ K and the relaxation time $\tau_{Te,relax}$ as a function of T_e at $n_e = 1.38 \times 10^{21}$ m^{-3} (the upper and lower horizontal scales are related in such a way that $n_{e\infty}$ is the Saha value at the corresponding value of $T_{e\infty}$).

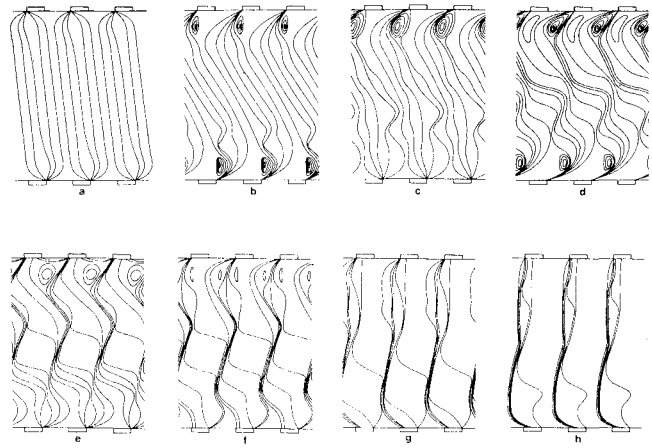

Fig. 7 Current streamline distribution shown at eight time instances before the constricted discharge structure is formed: a) $t = 0$, contour interval 0.082 A; b) $t = 1 \times 0.255$ μs, contour interval 0.095 A; c) $t = 2 \times 0.255$ μs, contour interval 0.103 A; d) $t = 3 \times 0.255$ μs, contour interval 0.114 A; e) $t = 4 \times 0.255$ μs, contour interval 0.114 A; f) $t = 5 \times 0.255$ μs, contour interval 0.226 A; g) $t = 6 \times 0.255$ μs, contour interval 0.448 A; g) $t = 8 \times 0.255$ μs, contour interval 0.992 A.

Hyperbolic Part

In order to follow the changes of n_e and T_e in time, Eqs. (4b) and (5c) must be solved simultaneously. The time step chosen should be small enough and is determined by the faster one of the changes n_e and T_e. In most discussions of the linearized theory[5] or numerical simulation[11] for the ionization instability, it is assumed that n_e is related to the electron temperature through the Saha equation, which means that n_e is assumed to relax instantaneously to its equilibrium value. However, for nonlinear calculations, the validity of this assumption must be checked from the values of the characteristic relaxation times of n_e and T_e for relaxation to the equilibrium values.

From the linear approximation the characteristic relaxation times for n_e and T_e are calculated by putting the initial value of n_e and T_e in the right-hand side of Eqs. (4b) and (5c), respectively.[6,9] Since these equations are nonlinear differential equations, it is possible that the real relaxation time is quite different from the one calculated by the above linear approximation. Therefore, we introduce the two relaxation times $\tau_{ne,\mathrm{relax}}$ and $\tau_{Te,\mathrm{relax}}$ which are obtained by numerically solving the nonlinear equations (4b) and (5c) in many practical cases as shown in Fig. 3.

In Fig. 4 the dotted line shows $\tau_{ne,\mathrm{relax}}$ for $n_{e0}=7.58\times10^{18}$ m^{-3} (which corresponds to the Saha equilibrium value at $T_e=2000$ K) as a function of n_e, keeping T_e constant at $T_{e\infty}$. The solid lines show $\tau_{Te,\mathrm{relax}}$ for various T_{e0} as functions of $T_{e\infty}$, keeping n_e constant at 7.58×10^{18} m^{-3}. The same relations of $\tau_{ne,\mathrm{relax}}$ and $\tau_{Te,\mathrm{relax}}$ for $n_{e0}=3.58\times10^{20}$ m^{-3} (Saha value at $T_e=3000$ K) and for $n_{e0}=1.38\times10^{21}$ m^{-3} (Saha value at $T_e=4000$ K) are shown in Figs. 5 and 6, respectively.

In all three cases $\tau_{Te,\mathrm{relax}} \ll \tau_{ne,\mathrm{relax}}$, which means that the electron temperature relaxation can be assumed to be instantaneous compared to the electron density relaxation. Hence, we will assume instantaneous temperature relaxation. Then Eq. (5c) is reduced to

$$\frac{2}{3kn_eT_e}\frac{j_x^2+j_y^2}{\sigma}-\delta m_e\left(1-\frac{T}{T_e}\right)\sum_{j=1}^{3}\frac{\nu_j}{m_j}-\left(1+\frac{2\mathcal{E}_i}{3kT_e}\right)\frac{\dot{n}_e}{n_e}=0 \tag{5d}$$

From this equation, the electron temperature T_e can be calculated by using the Newton-Raphson method.

Along the characteristic directions expressed by the following differential form,

$$\frac{dx}{dt}=u, \qquad \frac{dy}{dt}=0 \tag{30}$$

the continuity equation (4b) takes the form

$$\frac{dn_e}{dt}=k_f n_e(n_s-n_e)-k_r n_e^3 \tag{4c}$$

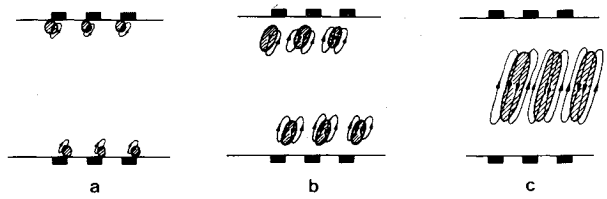

Fig. 8 Illustration of eddy currents: a) $t=0$; b) $t=2\div3\times0.255$ μs; c) $t=4\div5\times0.255$ μs (the dashed areas indicate regions with high conductivity).

It follows from Eq. (30), that if the relation

$$\Delta t=\Delta x/u \tag{31}$$

is satisfied, the electron density n_e can be calculated by the Runge-Kutta method from Eq. (4c).

The time step Δt must be chosen carefully. It must be larger than $\tau_{Te,\mathrm{relax}}$ to satisfy the condition $\partial T_e/\partial t=0$ and smaller than $\tau_{ne,\mathrm{relax}}$ to follow the change of n_e.

Putting $\Delta x=0.25$ mm and $u=980$ m/s into Eq. (31) we get $\Delta t=0.255$ μs. It can be seen from Figs. 4-6 that the above conditions are satisfied by using this value.

Results

Growth of Discharge Structure

The time history of the current distribution from $t=0$ to 8×0.255 μs is shown at different time steps in Fig. 7 (although

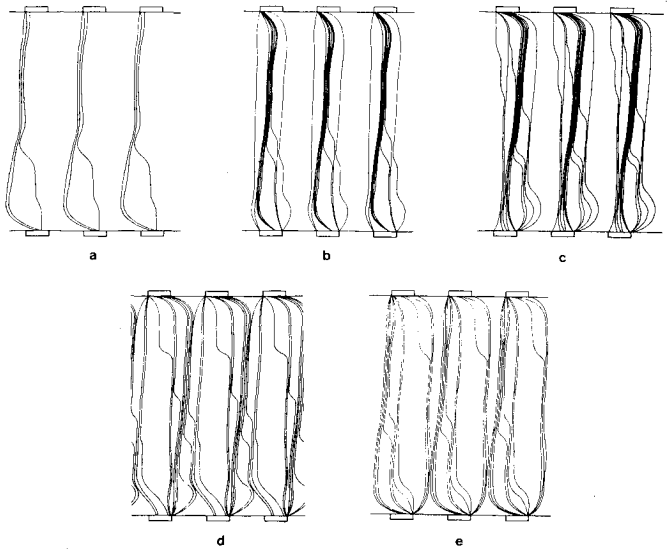

Fig. 9 Current streamline distribution at five time instances after the formation of the constricted discharge: a) $t=10\times0.255$ μs, contour interval 3.47 A; b) $t=20\times0.255$ μs, contour interval 3.26 A; c) $t=30\times0.255$ μs, contour interval 3.10 A; d) $t=40\times0.255$ μs, contour interval 3.40 A; e) $t=40\times0.255$ μs, contour interval 3.54 A.

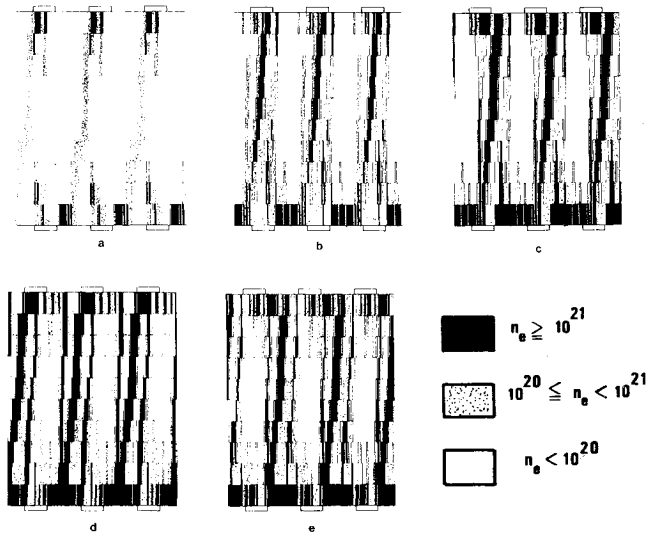

Fig. 10 Electron density distribution at five time instances after the formation of the constricted discharge structure: a) $t=10\times0.255$ μs; b) $t=20\times0.255$ μs; c) $t=30\times0.255$ μs; d) $t=40\times0.255$ μs; e) $t=50\times0.255$ μs.

Table 1 Value of T_e, n_e, σ, β, j_x, and j_y of elements 24-37 at $t=30\times0.255$ μs

	24	25	26	27	28	29	30	31	32	33	34	35	36	37
T_e	2783	2753	2572	2524	3332	3692	3985	4711	4760	3871	3663	3378	2712	2708
	2731	2792	2902	3244	3981	5124	5881	5736	4005	3199	2592	2799	2834	2746
	2809	2769	2626	3845	5116	5652	5810	5403	3176	2543	2724	2780	2660	2533
n_e	20	20	20	21	22	22	22	22	22	21	20	20	20	19
	0.150	0.132	0.125	0.554	0.135	0.161	0.162	0.162	0.136	0.177	0.169	0.105	0.118	0.842
σ	2	2	2	3	3	3	3	3	3	2	2	1	2	1
	0.137	0.118	0.106	0.181	0.282	0.309	0.300	0.303	0.284	0.924	0.164	0.952	0.105	0.787
β	17.2	16.8	16.0	6.14	3.92	3.60	3.46	3.49	3.90	9.75	18.2	16.9	16.6	17.5
j_x	3	3	3	4	5	5	5	5	5	4	4	4	4	3
	0.650	0.404	0.605	−0.975	−0.256	−0.307	−0.282	−0.261	−0.186	−0.461	0.136	0.135	0.124	0.748
j_y	4	4	4	6	6	6	6	6	6	6	4	4	4	4
	0.497	0.493	0.569	−0.151	−0.304	−0.370	−0.378	−0.358	−0.306	−0.101	0.410	0.380	0.464	0.284

the calculation is done in one segment, three segments are shown in the figures). The nonlinear growth of the discharge structure caused by the ionization instabilities is clearly seen from this set of figures. It should be noted that the contour interval of these figures is different for each time step and increases rapidly with time.

The current concentrated parts at $t=0$ near the electrode edges on the anode and cathode will become regions of relatively high conductivity. Both regions are convected downstream at the next time $t=1\times0.255$ μs, which causes the asymmetrical current distributions at subsequent times. Due to the large conductivity gradient, the eddy currents will flow as illustrated in Fig. 8a which leads to the current distributions at $t=1\times0.255$ μs shown in Fig. 7b.

After a few time steps at $t=2$ or 3×0.255 μs, the relatively high-conductivity region spreads out, creating eddy currents as shown in Fig. 8b. The eddy currents have negative x and y components in the high-conductivity region since both E_x^* and E_y^* are negative in the channel. Hence the current distributions at these two instances become as illustrated in Fig. 7c or 7d.

The high-conductivity region becomes larger during the next few time steps and at $t=4$ or 5×0.255 μs it produces large eddy currents as shown in Fig. 8c which result in constricted structures in the center of the channel shown in Figs. 7e and 7f.

The constricted part extends toward the electrodes and interconnects the anode and the cathode, finally forming streamers at $t=6$ and 8×0.255 μs, the electron density and current density in the streamers are of order 10^{20} m^{-3} and of order 10^4 A/m^2, respectively.

It is interesting to see that the constricted discharge structure inclines about 45 deg from the original current flow direction when the current constricts only in the center of the channel (compare Fig. 7e with Fig. 7b) and that the angle decreases in time since the discharge structure will be influenced by the boundary conditions at the constricted part extends to the electrodes (see Fig. 7h).

Streamer Development

The time history of the current and the electron density distributions after the streamers are formed until they are fully developed is illustrated at five time instances ($t=10$, 20, 30, 40, and 50×0.255 μs) in Figs. 9 and 10, respectively. In Fig. 9, the contour interval is taken nearly equal in five cases. The current concentrations due to the shorting of the Hall field always occur at the upstream edge of the anode and the downstream edge of the cathode. These concentrations will produce regions of high electron density, which are convected downward along the electrode on the anode side and along the insulator on the cathode side and which will contribute to further current concentrations on the anode but not on the cathode. This causes the higher electron density on the anode side than the cathode side in Fig. 10. Electron temperature distributions at $t=30\times0.255$ μs are shown in Fig. 11. The values of electron density, electron temperature, conductivity, Hall parameter, and current density corresponding to the elements shown in Fig. 12 are listed in Table 1.

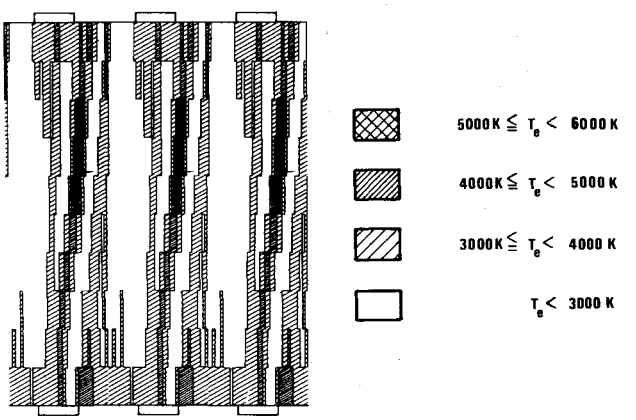

Fig. 11 Electron temperature distribution at $t=30\times0.255$ μs.

From Figs. 9, 10, and 12 and Table 1, the following characteristics become clear:

1) High current density, high electron density, and high electron temperature regions are strongly interconnected.

2) After the streamers are formed, they are frozen in the gas and are convected downstream at the gas velocity.

3) Streamers move smoothly from one electrode pair to the next and when they are located in the transient region of two sections, they are electrically connected to two adjacent electrodes.

4) At the instant the streamers are formed ($t=10\times0.255$ μs) the electron density in the streamers is of order 10^{20} m^{-3} and increases in time until the cesium is fully ionized.

5) The electron temperature in the streamers is between 4000 and 6000 K.

6) Outside the streamers, the electron density is of order 10^{19} m^{-3} and the electron temperature between 2000 and 3000 K.

7) The streamer angle is somewhat in the direction of the negative x axis.

8) Near the electrodes, the streamers are more irregular than in the bulk region.

Table 2 List of the nine terms in electron continuity and electron equations of elements 24-37 at $t=30\times0.255$ μs

	24	25	26	27	28	29	30	31	32	33	34	35	36	37
C_1	5	5	5	5	5	4	4	3	5	5	4	5	5	5
	1.42	1.91	3.14	2.40	1.77	9.16	1.28	−6.71	1.69	8.34	6.73	1.98	2.32	1.54
C_2	4	4	5	5	5	4	3	4	5	5	5	4	4	4
	2.14	3.56	−7.31	−9.17	−2.09	−3.65	−1.94	3.43	4.34	8.60	5.53	7.07	4.38	3.79
C_3	6	6	6	6	6	6	6	6	6	6	6	6	6	6
	2.16	2.71	4.07	5.95	2.97	2.63	2.42	2.20	2.93	9.45	1.25	2.50	3.18	2.30
C_4	5	5	5	5	6	6	6	6	6	5	5	5	5	5
	−4.50	−4.71	−5.12	−9.08	−1.47	−2.02	−2.40	−2.32	−1.48	−7.18	−4.02	−4.72	−4.86	−4.51
C_5	6	6	6	6	6	5	4	4	6	6	5	6	6	6
	−1.70	−2.25	−3.57	−2.47	−1.51	−6.29	−7.85	4.19	−1.44	−8.67	−8.49	−2.32	−2.70	−1.84
C_6	4	4	5	5	5	4	3	4	5	5	5	4	4	4
	1.43	2.38	−4.88	−6.12	−1.39	−2.43	−1.29	2.28	2.89	5.73	3.69	4.71	2.92	2.53
C_7	4	4	4	5	5	5	4	5	5	4	4	3	3	3
	−4.72	−1.59	−3.38	−1.15	−1.67	−1.43	−4.10	1.38	2.06	3.31	2.10	−5.28	2.03	4.17
C_8	2	2	3	4	4	4	4	3	4	4	4	3	2	3
	−4.01	−2.82	−1.23	1.64	1.26	1.28	1.14	3.92	−1.18	−3.11	1.15	9.17	9.91	2.93
C_9	4	3	3	4	4	4	5	5	5	4	4	3	3	2
	−1.53	2.00	9.94	4.32	6.71	−6.85	−1.65	−2.90	1.54	1.39	3.07	−6.96	−5.08	−1.18

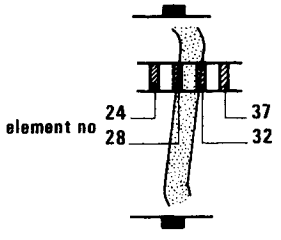

Fig. 12 Location of elements considered in Table 1.

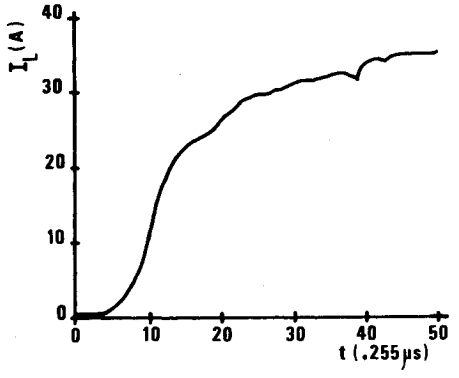

Fig. 13 Time dependence of the load current I_L.

These results agree quite well with the experimental results obtained from the shock-tube facility.[3]

Characteristic Time

Figure 13 shows the time dependence of the load current I_L. The characteristic relaxation time of load current is about 10 μs in which the gas moves 1 cm along the channel. This value agrees with the characteristic growth time of an individual streamer determined from streak pictures taken during shock-tube experiments.

Global Parameters

The global parameters at time $t=50\times0.255$ μs are as follows: load current $I_L=35.4$ A, load voltage $V_L=70.7$ V, average power density $P_d=156$ MW/m^3, load factor $K=0.602$, effective conductivity $\sigma_{\text{eff}}=75.6$ S/m and effective Hall parameter $\beta_{\text{eff}}=2.4$. These values show a good generator performance. This means that after the relaxation region the generator performs well even under nonuniform conditions.

Validity of Simplified Equations

The two terms in the electron continuity equation (4b)

$$C_1=\frac{\dot{n}_e}{n_e}=k_f(n_s-n_e)-k_r n_e^2, \qquad C_2=\frac{u}{n_e}\frac{\partial n_e}{\partial x}$$

and the seven terms in electron energy equation (5b)

$$C_3=\frac{2}{3kn_eT_e}\frac{j_x^2+j_y^2}{\sigma} \qquad C_7=\frac{5}{3}\left(u-\frac{j_x}{n_ee}\right)\frac{1}{T_e}\frac{\partial T_e}{\partial x}$$

$$C_4=\delta m_e\left(1-\frac{T}{T_e}\right)\sum_{j=1}^{3}\frac{\nu_j}{m_j} \qquad C_8=\frac{5}{3}\frac{j_x}{n_ee}\frac{1}{T_e}\frac{\partial T_e}{\partial y}$$

$$C_5=\left(1+\frac{2\mathcal{E}_i}{3kT_e}\right)\frac{\dot{n}_e}{n_e} \qquad C_9=\frac{2}{3}\frac{1}{n_ekT_e}\nabla\cdot q_e$$

$$C_6=\frac{2}{3}\frac{u}{n_e}\frac{\partial n_e}{\partial x}$$

are calculated for each element in Fig. 12 and are listed in Table 2. For the calculation of the heat conduction term C_9, the following relation is used:

$$\nabla\cdot q_e=\frac{3}{2}\frac{k}{m_e}\frac{T_e}{\nu_e}\frac{1}{1+\beta^2}\left(\frac{\partial^2 T_e}{\partial x^2}+\frac{\partial^2 T_e}{\partial y^2}\right)$$

It is clear from Table 2 that the Joule heating term C_3 in the electron energy equation is always of order 10^6. Further, of the other six terms, either the collision loss term C_4 or the ionization-recombination term C_5 is of order 10^6 and at least one order larger than the other four terms C_6, C_7, C_8, and C_9.

Conclusions

A two-dimensional, time-dependent numerical model of a partially ionized, highly magnetized MHD plasma has been discussed. The following conclusions are derived from our calculations:

1) The electron temperature relaxation time is much shorter than the electron density relaxation time.

2) The constricted discharge structure is formed within 2 μs as the result of nonlinear growth of ionization instabilities.

3) After the formation of a streamer, n_e grows until the condition of a fully ionized seed has been reached.

4) The characteristic growth time of a streamer is about 10 μs.

5) The streamers are frozen in the gas and are convected downstream with the gas velocity.

6) The electron temperature in the streamers is between 4000 and 6000 K.

7) Outside of the streamers, the electron density is of order 10^{19} m^{-3} and the electron temperature between 2000 and 3000 K.

8) For the conditions considered, the effective conductivity and Hall parameter are 75 S/m and 2.4, respectively, and the average power density is 156 MW/m^3 which means that after the relaxation region the generator performance is good.

Acknowledgment

This work was performed with financial support from the Nederlandse Organisatie voor Zuiver-Wetenschappelijk Onderzoek (ZWO).

The authors wish to thank Drs. J. H. Blom and A. J. Mesland for stimulating and useful discussions. The authors also wish to acknowledge the excellent service of the operators of the University Computer Center.

References

[1] Zauderer, B., "Discharge Structure and Stability of a Nonequilibrium Plasma in a Magnetohydrodynamic Channel," *Physics of Fluids,* Vol. II, 1968, pp. 2577-2585.

[2] Brederlow, G., Witte, K. J., and Zinko, H., "Investigations of the Discharge Structure in a Noble Gas Alkali MHD Generator Plasma, Parts I and II," *AIAA Journal,* Vol. 11, 1973, pp. 1065-1079.

[3] Veefkind, et al., "Investigation of the Nonequilibrium Condition in a Shock-Tunnel Driven Noble Gas MHD Generator," *Proceedings of VIIth International Conference on Electric Power Generation,* Cambridge, Mass., Vol. II, 1980, pp. 703-710.

[4] Mitchner, M. and Zampaglione, V., "The Ionization Instability in the Nonlinear Regime," *Proceedings of 12th Symposium on Engineering Aspects of MHD,* Argonne, Ill, 1972, pp. V.8.1 ~ V.8.6.

[5] Solbes, A., "Quasi-Linear Plane Wave Study of Electrothermal Instabilities," *Proceedings of IVth International Conference on MHD Electric Power Generation,* Warsaw, Vol. 1, 1968, pp. 499-518.

[6] Nelson, A. H. and Haines, M. G., "Analysis of the Nature and Growth of Electrothermal Waves," *Plasma Physics,* Vol. 11, 1969, pp. 811-837.

[7] Hower, N. L. and Mitchner, M., "Nonlinear Calculations of the Effective Conductivity of Inhomogeneous MHD Generator Plasmas," *Proceedings of VIth International Conference on MHD Electric Power Generation,* Washington, D. C., Vol. IV, 1975, pp. 217-236.

[8] Martinez Sanchez, M., de Saro, R., and Louis, J. F., "Effective Ohm's Law for a Class of Inhomogeneous Plasmas and Its Effect on the Performance of Combustion Driven MHD Generators," *Proceedings of VIth International Conference on MHD Electric Power Generation,* Washington, D. C., Vol. IV, 1975, pp. 247-264.

[9] Lengyel, L. L., "Numerical Simulation of Ionization Instability with Allowance for Dissipative Processes," *Proceeding of 11th Symposium on Engineering Aspects of MHD,* Pasadena, Calif., 1970, pp. 193-198.

[10] Velikhov, E. P., Degerev, L. M., Samarskii, A. A., and Favorskii, A. P., "Numerical Experiment on Ionization Instability Development in a Low Temperature Magnetized Plasma," *Proceedings of 10th Symposium on Engineering Aspects of MHD,* Cambridge, Mass., 1969, pp. 1-4.

[11] Uncles, R. J., "A Numerical Investigation of the Current and Density Distributions for a Nonequilibrium Plasma in a Segmented Electrode Duct," *Plasma Physics,* Vol. 15, 1973, pp. 1053-1065.

[12] Hara, T. and Umoto, J., "Three-Dimensional Effects of Electrode Configuration on Diagonal MHD Generator Performance," *Journal of Energy,* Vol. 3, Jan.-Feb. 1979, pp. 16-22.

[13] Spitzer, L., *Physics of Fully Ionized Gases,* Interscience Publishers, New York, 1956.